Actin-binding proteins sensitively mediate F-actin bundle stiffness

MIREILLE M. A. E. CLAESSENS[1]*, MARK BATHE[2]*, ERWIN FREY[2] AND ANDREAS R. BAUSCH[1†]

[1]Lehrstuhl für Biophysik-E22, Department of Physics, Technische Universität München, D-85748 Garching, Germany

[2]Arnold Sommerfeld Center for Theoretical Physics and CeNS, Department of Physics, Ludwig-Maximilians-Universität München, D-80333 Munich, Germany

*These authors contributed equally to this work

[†]e-mail: abausch@ph.tum.de

Published online: 20 August 2006; doi:10.1038/nmat1718

Bundles of filamentous actin (F-actin) form primary structural components of a broad range of cytoskeletal processes including filopodia, sensory hair cell bristles and microvilli. Actin-binding proteins (ABPs) allow the cell to tailor the dimensions and mechanical properties of the bundles to suit specific biological functions. Therefore, it is important to obtain quantitative knowledge on the effect of ABPs on the mechanical properties of F-actin bundles. Here we measure the bending stiffness of F-actin bundles crosslinked by three ABPs that are ubiquitous in eukaryotes. We observe distinct regimes of bundle bending stiffness that differ by orders of magnitude depending on ABP type, concentration and bundle size. The behaviour observed experimentally is reproduced quantitatively by a molecular-based mechanical model in which ABP shearing competes with F-actin extension/compression. Our results shed new light on the biomechanical function of ABPs and demonstrate how single-molecule properties determine mesoscopic behaviour. The bending mechanics of F-actin fibre bundles are general and have implications for cytoskeletal mechanics and for the rational design of functional materials.

The mechanical requirements of F-actin bundles are intimately connected to the specific biological function that they are designed to fulfil. Bundles integrated into the cytoskeleton are designed principally to reinforce the cell against mechanical deformation, highly dynamic filopodia present at the leading edge of motile cells are needed to exert potentially large protrusive forces against the advancing membrane during phagocytosis or migration through the dense extracellular space[1–3], whereas microvilli are passive structural elements that serve primarily to increase the apical surface area of intestinal epithelial cells, thereby enhancing diffusive nutrient transport. In each case, the cell uses specific ABPs to bundle F-actin and carry out its biological function. α-actinin predominates in cytoskeletal bundles and muscle[4], fascin is prevalent in filopodia[5,6], and plastin is predominant in microvilli and stereocilia[7,8]. The disparate mechanical requirements of these cellular processes, together with the broad evolutionary conservation of their predominant ABPs across vertebrate and invertebrate eukaryotes, suggests that a key component of ABP biological function is its ability to differentially mediate F-actin bundle stiffness[9]. A mechanistic understanding of the effects of ABPs on F-actin bundle mechanics might thus be needed to obtain a complete understanding of their physiological role in cells[10–12]. Quantifying the governing mechanical principles of these fundamental cytoskeletal constituents should also prove valuable in the design of biomimetic nanomaterials[13].

F-actin bundles can be characterized mechanically by their intrinsic bending stiffness, κ_B, which is related to their persistence length, l_p, in the same manner as for any polymer, $\kappa_B = l_p k_B T$. Here, l_p is the length scale over which associated thermal fluctuations destroy memory of a direction initially tangent to the bundle backbone and $k_B T$ denotes thermal energy, where k_B is the Boltzmann constant and T is absolute temperature. κ_B is the mechanical property of interest for F-actin bundles because it can be used to calculate, for example, the maximal force that can be exerted by filopodia before buckling[2,3,14] or mechanotransduction mechanisms of brush-border microvilli[15] and hair-cell stereocilia[16,17].

Two limiting types of F-actin bundle bending with notably different associated κ_B have been reported (Fig. 1)—decoupled bending, in which constituent actin filaments bend independently because intervening crosslinks do not resist shear and instead

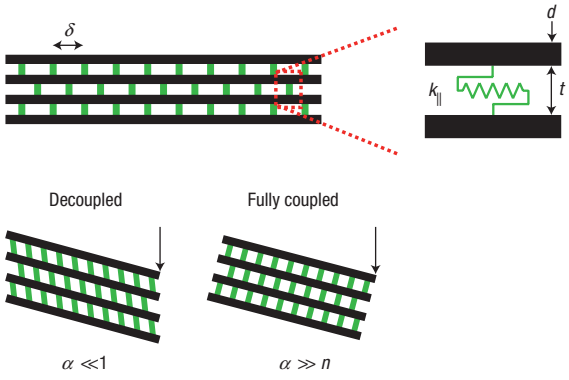

Figure 1 F-actin bundle model. F-actin filaments (black) are coupled to nearest-neighbour filaments by discrete ABPs (green) with axial spacing, δ (m), and shear stiffness, $k_\parallel$ (N m^{-1}). F-actin is characterized mechanically by its backbone extensional stiffness, $k_a = EA/L_B$, where $EA = 4.4 \times 10^{-8}$ N (ref. 26), length L_B, and bending stiffness, $\kappa_B = EI = 7.3 \times 10^{-26}$ N m^2 (ref. 37), where E is the effective Young's modulus, A is the effective cross-sectional area, and I is the second moment of the cross-sectional area of F-actin. The interfilament spacing, t, is fixed by the length of the intervening ABPs and remains constant in tightly crosslinked bundles. The ratio, $\alpha \equiv k_\parallel L_B / k_a \delta$, mediates a competition between crosslink shearing and F-actin filament extension or compression during bundle bending, which determines the bundle bending regime (see text for details).

'tilt' freely during bundle bending[18,19], and fully coupled bending, in which filaments are rigidly 'glued' together by intervening crosslinks that strongly resist shear, forcing filaments away from the bundle neutral surface to additionally stretch or compress during bending. The former scenario results in a simple linear dependence of κ_B on the number of filaments, n, constituting the bundle. This scaling is what is expected when bending a loose stack of paper and has been observed in the sensory hair bundles of the frog sacculus, where the ABP plastin is predominant[18]. In contrast, the latter scenario results in a much stronger quadratic dependence, $\kappa_B \sim n^2$, identical to the result for a standard homogeneous mechanical beam, as would be expected if the sheets of paper were glued rigidly together to prohibit interlayer shear deformation. This fully coupled regime was measured quantitatively for the crystalline actin bundle found in the acrosomal process of horseshoe crab sperm cells at fully saturated scruin:actin concentrations[20]. Thus, ABP type clearly affects the degree of shear coupling between F-actin filaments and consequently κ_B. However, it is not obvious *a priori* what role specific molecular properties such as ABP shear and extensional stiffness, molecular length, and concentration play in mediating the associated bundle bending regime.

To address these questions, we systematically investigate the dependence of κ_B on bundle size and ABP type and concentration using an emulsion droplet system[21]. Briefly, actin is polymerized in the water phase of a water–dodecane emulsion. The emulsion droplets are stabilized with phospholipids to prevent coagulation and mimic the presence of a fluid membrane with essentially no bending undulations. In the absence of bundling proteins, this procedure results in isolated emulsion droplets containing entangled F-actin solutions that can be observed directly using fluorescence microscopy (Fig. 2a). Small droplets in the absence of ABPs were used to obtain the filament density or equivalently the total contour length of F-actin, at a given actin concentration, c_a. Inclusion of ABPs such as fascin, plastin, or α-actinin in the polymerization process results in a single compact F-actin bundle formed into a closed ring that is thermally fluctuating (Fig. 2b). The total contour length of F-actin in any given droplet is given solely by the droplet volume and the actin concentration. Thus, the total bundle thickness can be calculated from the determined filament density and the ring radius. As demonstrated theoretically by Odijk[22], the amplitude of the transverse thermal fluctuations of the ring backbone, D_B, is determined at any given temperature solely by κ_B and the radius, R_c, of the ring, $\kappa_B = 0.16 k_B T R_c^3 / D_B^2$ (Fig. 2b and Methods section). Systematic variation of droplet volume and actin–ABP concentrations in the microemulsion system allows, for the first time, the controlled investigation of the dependence of κ_B on n for each ABP considered (Fig. 2).

For each ABP type and concentration examined, κ_B depends strongly on n and converges to the expected single-filament value of 7×10^{-26} N m^2 ($l_p = 17 \times 10^{-6}$ m at $T = 298$ K)[23] (Fig. 3). Differences in the dependencies of κ_B on n for the different ABP types and concentrations, c_{ABP}, however, are drastic. The κ_B of plastin-crosslinked bundles increases linearly with n independently of $c_{plastin}$ (for $c_{plastin}/c_a \leq 0.5$) (Fig. 3a), whereas the κ_B of fascin-crosslinked bundles depends strongly on both n and c_{fascin} (Fig. 3b).

The linear scaling exhibited by κ_B for plastin-crosslinked bundles is consistent with the decoupled bending scenario in which F-actin filaments contribute equally and independently to κ_B (Fig. 1), even at high $c_{plastin}$:c_a. We postulate that the physical origin of this observation is that plastin is too weak to resist the interfilament shear deformation associated with decoupled bundle bending, which is consistent with the crosslink tilting observed in plastin–F-actin bundles using electron microscopy[19,24]. Additional support for this hypothesis is provided by the dependence of κ_B on n and c_{fascin}, which is quantitatively explained by a purely mechanical model of fibre bundle bending that accounts for the interplay between F-actin filament stretching and interfilament ABP shearing[25] (see the Methods section).

In this mechanical model, F-actin is treated as a standard Euler–Bernoulli beam that is capable of extension/compression in addition to pure bending[25] (Fig. 1 and Methods section). Crosslinking ABPs mechanically couple neighbouring filaments during bundle bending by resisting interfilament shear with shear stiffness, $k_\parallel$. ABP–actin binding affinity and c_{ABP} in the droplet then determine the mean axial spacing of ABPs in the bundle, δ, via chemical equilibrium, which gives rise to an overall effective shear stiffness coupling neighbouring filaments, $k_\parallel/\delta$. The single unknown parameter in the model, $k_\parallel$, is an intrinsic property of any ABP that is a result of protein structure and binding geometry. The bending stiffness of fascin-crosslinked F-actin filaments can be fitted uniquely as a function of both n and c_{fascin} using $k_\parallel = 3 \times 10^{-5}$ N m^{-1} (Fig. 2b). The plastin-concentration-independence of κ_B allows only an upper bound of $k_\parallel \leq 0.1 \times 10^{-5}$ N m^{-1} to be calculated.

The crossover in κ_B from n^2 scaling to n scaling has its origin in the finite shear stiffness of the crosslinks. The mechanical model predicts that κ_B must eventually crossover from n^2 scaling to n scaling with increasing n due to a competition between crosslink shearing and F-actin filament stretching/compression. Indeed, agreement between the model and experimental data for fascin suggests that this crossover is observed at all but the lowest concentration examined, where a fully coupled n^2 scaling at low n is superseded by linear scaling at higher n (Fig. 3b). This crossover originates from the fact that to maintain n^2 scaling, each filament that is successively added to the outer shell of the bundle must be extended/compressed proportionately because the axial strain field in a fully coupled bundle varies linearly across the cross-section. The increasing energetic cost of adding filaments to the bundle in this manner must therefore eventually outweigh the cost of shearing the crosslinks instead, which is

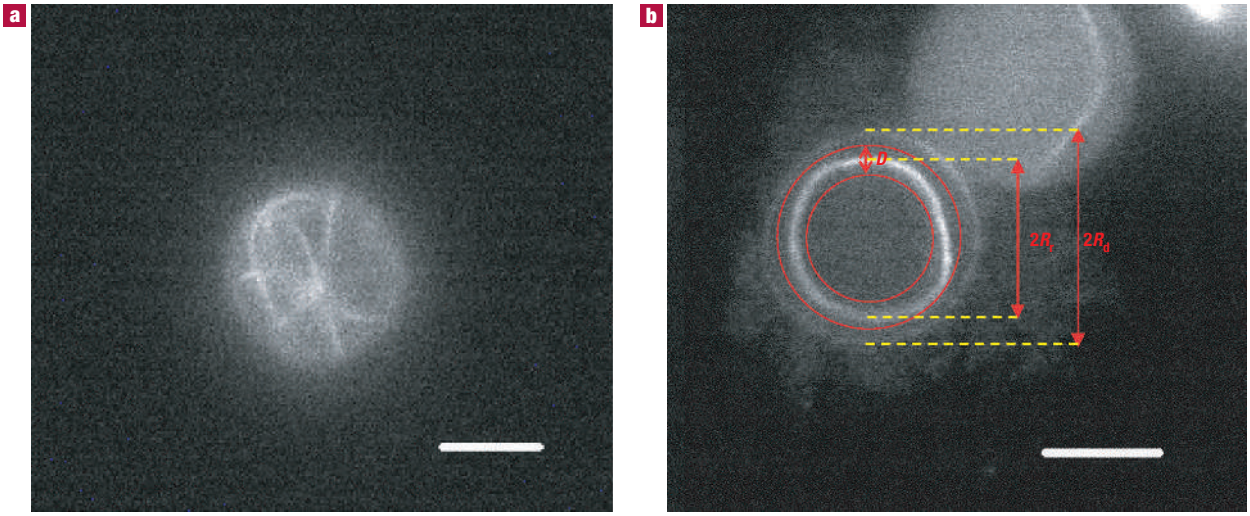

Figure 2 Experimental setup. a, Isolated F-actin filaments polymerized in an emulsion droplet in the absence of ABPs form a random isotropic solution. **b**, Inclusion of ABPs in the polymerization process leads to the formation of a single F-actin bundle that organizes into a ring of root-mean-square radius, R_r. Actin concentration, c_a, and droplet volume, $V_d = 4\pi R_d^3/3$, where R_d is the droplet radius, determine the total length of F-actin present in the droplet and thus the number of filaments, n, constituting the bundle. The experimentally determined filament density was in good agreement with the total length obtained directly from the number density of actin monomers. Thermal fluctuations of the bundle backbone are characterized by the fuzzy diameter, D, which is directly related to κ_B (see the Methods section). The scale bars are 10 μm.

independent of bundle thickness. At that point, crosslink shearing relieves filament stretching/compression, leading directly to the crossover in κ_B from fully coupled n^2 scaling to n scaling. This regime is shear-dominated and intermediate to the fully coupled and decoupled regimes. The fact that the crossover in κ_B occurs at decreasing n with decreasing fascin concentration (Fig. 3b) is consistent with this picture because it is the effective shear stiffness, $k_\parallel/\delta$, that denotes the strength of the shear coupling. A scaling analysis that evaluates the energetic costs of crosslink shearing and fibre stretching suggests that the dimensionless quantity, $\alpha \equiv k_\parallel L_B/k_a\delta$, denotes the relevant bundle bending regime, where $(\alpha \gg n)$, $(\alpha \ll 1)$ and $(1 \ll \alpha \ll n)$ for the fully coupled, decoupled and shear-dominated regimes, respectively. L_B is the bundle length and $k_a = EA/L_B$ is the axial stretching stiffness of F-actin, where $EA = 4.4 \times 10^{-8}$ N (ref. 26). This scaling result is generally applicable to any crosslinked fibre bundle provided that k_a is substituted with the appropriate stretching stiffness of the constituent fibre[27].

Increasing the length of the crosslinker shifts the crossover in κ_B to lower n because the energetic cost associated with filament stretching/compression in fully coupled bending is proportional to the distance of the filament to the centre of the bundle. This effect is observed for α-actinin (Fig. 3c), which has a molecular length that is roughly three times that of fascin. As a result, the crossover only occurs at $n \approx 3$–4 and a relatively large associated shift in κ_B is observed. Fitting the model to the data yields $k_\parallel = 2.5 \times 10^{-5}$ N m^{-1}.

Depletion forces induced by small molecules present in the cytosol may also act as effective crosslinkers that bundle F-actin, as demonstrated *in vitro* using polyethylene glycol[28,29] (PEG). To examine the potential role of depletion forces on F-actin bundle stiffness, we also measured κ_B in the presence of PEG (molecular mass 6 kDa, 2 and 4 w/w%). Interestingly, κ_B depends quadratically on n for the entire range of n examined (Fig. 3d), indicating that the bundle remains in the fully coupled regime for all bundle sizes investigated ($n < 30$). This places a lower bound on PEG's effective crosslinking shear stiffness per unit length of $k_\parallel/\delta \geq 10^3$ N m^{-2}. This value can be compared directly to the ABPs examined assuming $\delta = 10^{-7}$ m, the typical ABP axial spacing at high ABP concentration, which results in $k_\parallel \geq 10^{-4}$ N m^{-1}. We postulate that this relatively high stiffness has its origin in a tight intermolecular packing of the helical F-actin filaments that prohibits interfilament slip. Given that depletion forces induce fully coupled bundle bending, an important functional role of ABPs *in vivo* might actually be to prevent fully coupled bending by acting as interfilament spacers.

Folded proteins have complex, anisotropic mechanical properties that depend strongly on secondary and tertiary structure, the magnitude of applied deformations and the length scales probed[30]. In our experiments thermal fluctuations of the bundle backbone result in ABP shear strains of the order of only 1%. Thus, ABPs are only deformed on the ångström scale, and the observed shear stiffness may be expected to be considerably lower than the extensional stiffness probed by single-molecule unfolding experiments (10^{-3}–10^0 N m^{-1}) typically with nanometre resolution[31,32]. The hierarchical structure of proteins allows for a nonlinear mechanical response: a soft response at small deformations is possible without compromising protein stability. Detailed molecular simulations are required to elucidate the precise origin of the observed ABP shear stiffness. However, it is important to note that in our equilibrium thermodynamic analysis we determine an effective shear stiffness. ABPs have finite on/off rates that set the binding stoichiometry or average number of bound ABPs used in our analysis (see the Methods section). Thus, the effective shear stiffness determined for each ABP contains these binding/unbinding effects.

Living cells use a limited number of ABPs to tightly crosslink F-actin filaments into bundles, and a single ABP type can predominate a given cytoskeletal process. The values of ABP shear stiffness observed here can be used together with the known lengths of physiological bundles to determine the dimensionless parameter, α, and thus the associated bending regime for F-actin bundles found in nature. The decoupled bending regime clearly indicates a mechanical preference for maximal bundle compliance, the fully coupled regime for maximal bundle stiffness, whereas the shear-dominated regime could indicate a preference for an

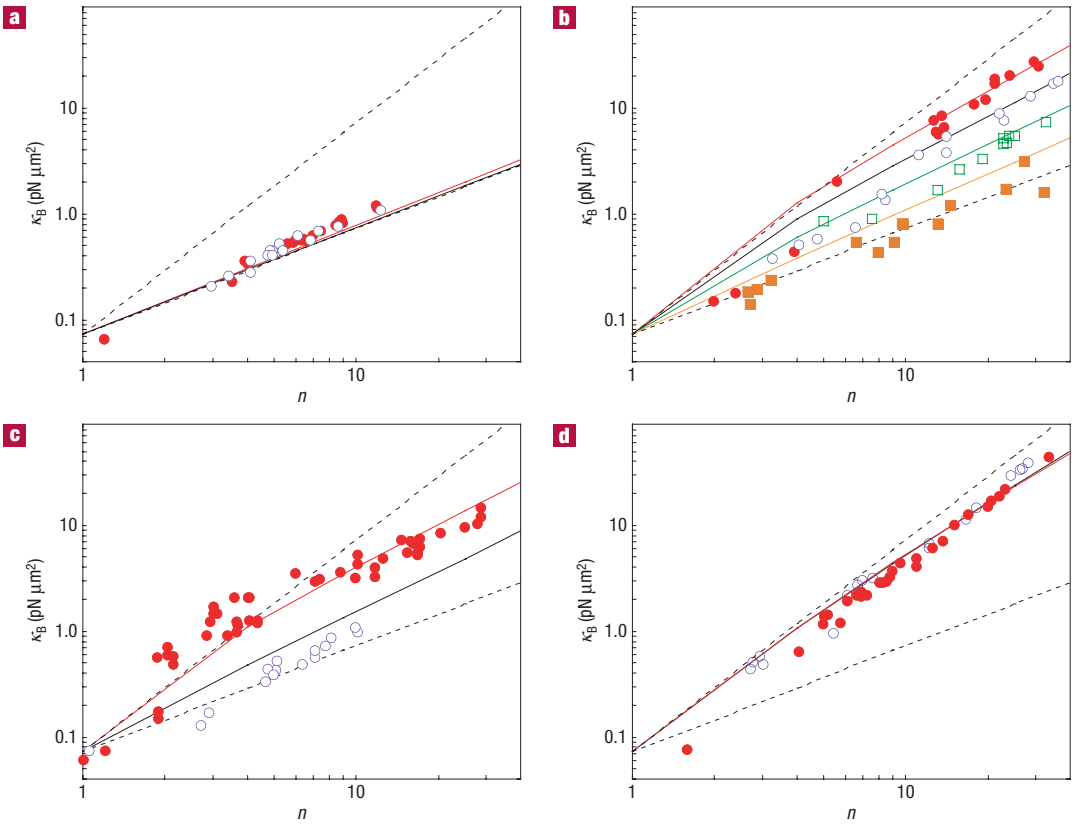

Figure 3 F-actin bundle bending stiffness, κ_B. **a**, Bundles crosslinked by plastin exhibit linear scaling in the number of filaments, n, constituting the bundle for both low (open circles—1:50) and high (filled circles—1:2) crosslinker:actin concentration ratios, $r_{ABP:a}$. **b**, κ_B for fascin-crosslinked bundles depends strongly on fascin concentration, c_{fascin}, in addition to bundle size ($r_{ABP:a}$ filled circles—1:2, open circles—1:5, open squares—1:20, filled squares—1:50). Deviations of the model from experiment at small bundle sizes ($n \leq 6$) are attributed to the disordered bundle structure probably present in that regime, which is not accounted for theoretically. **c**, The molecular length of α-actinin is considerably longer than that of fascin or plastin (35 nm versus 10 nm) but has a shear stiffness similar to that of fascin (see text), $r_{ABP:a}$ filled circles—1:10, open circles—1:50. **d**, F-actin filaments bundled non-specifically by PEG-induced depletion forces (4% PEG6k—filled circles, 2% PEG6k—open circles) exhibit a κ_B that increases quadratically in n to large bundle sizes ($n \sim 30$), yielding a lower bound on the effective crosslinker stiffness per unit length of $k_\parallel / \delta \geq 10^3$ N m^{-2}. The dashed lines indicate decoupled ($\alpha \ll 1$; $\kappa_B = n\kappa_a$) and fully coupled ($\alpha \gg n$; $\kappa_B = n^2\kappa_a$) bundle bending regimes assuming zero interfilament spacing ($t = 0$). The determination of the total F-actin length results in a relative error of ∼10% in n.

actively tunable bundle stiffness that may be varied between the two limits by varying ABP concentration or bundle size. For example, plastin is predominant in brush-border microvilli, which range from 2 to 5 µm in length and consist of 20–30 filaments. Thus, they are in the decoupled bending regime, which could have important biological consequences. Interestingly, owing to the filopodia lengths typically observed, even their bending response is expected to be in this regime. However, it is re-emphasized that we only explore the linear, small deformation shear response of ABPs in this work and nonlinear ABP shear response may be important. A biological advantage of the observed soft shear stiffness of ABPs could be that distinct mechanical response regimes can be fully exploited depending on the magnitude of bundle deformations. The hierarchical stiffness of proteins and their highly nonlinear response provides an additional means of tuning the bending stiffness of F-actin bundles. It remains a formidable challenge to explore the nonlinear mechanical response of such bundle structures.

Finally, the results presented here highlight the importance of using *in vitro* systems to determine the biomechanical function of ABPs, especially considering the practical difficulties associated with *in vivo* experiments. Comparing the mechanical properties of bundles formed using a range of ABPs, we demonstrate that bundle mechanics are defined by single-molecule properties. It is the formidable challenge of understanding the relationship between single-molecule structure, mechanics, and the collective behaviour of their macromolecular assemblies that is necessary to bridge the existing gap in our understanding of biologically important processes[10–12]. The governing principles of bundle bending elucidated in this investigation are completely general and are as equally applicable to fibre bundles of microtubules or carbon nanotubes as they are to bundles of F-actin. We isolated the dimensionless bundle bending stiffness parameter, α, which may be used in the future to rationally design biological and biomimetic (nano-)materials that use fibre bundles for enhanced structural stiffness, by tuning the associated bundle bending regime and hence the associated bending stiffness by orders of magnitude.

METHODS

PROTEIN PREPARATION

α-actinin is isolated from turkey gizzard smooth muscle[33], dialysed against G-buffer (2 mM Tris, 0.2 mM ATP, 0.2 mM $CaCl_2$, 0.2 mM dithiothreitol, 0.005% NaN_3) and stored at 4 °C for several weeks. Recombinant plasmids containing either the full-length human I-plastin cDNa (a kind gift from F. Rivero, Köln, Germany) or human fascin (a kind gift from D. Vignjevic,

Paris, France) are transformed in *Escherichia coli* L12-codon+bacteria. *E. coli* bacteria carrying the plasmid are grown at 37 °C until the absorbance of the culture at 600 nm, A_{600}, reached 0.6. Protein expression is induced with isopropyl-β-*D*-thiogalactopyranoside at 37 °C for I-plastin and at 20 °C for fascin. G-actin is extracted from rabbit skeletal muscle[34]. Lyophilized G-actin is dissolved in deionized water and dialysed against G-buffer at 4 °C for 24 h. Solutions of G-actin are kept at 4 °C and used within 7 days of preparation. Emulsion droplets are stabilized with phospholipids (95 mol% DOPG (1, 2-dioleoyl-*sn*-glycero-3-[phospho-*rac*-(1-glycerol)]), 5 mol% DMPE-PEG2000 (1, 2-dimyristoyl-*sn*-glycero-3-phosphoethanolamine-N-[Methoxy(Polyethylene glycol)-2000], Avanti Polar Lipids)). DMPE-PEG2000 prevented adsorption of filaments and ABPs to the droplet wall[35]. F-actin is fluorescently labelled with phalloidin-tetramethylrhodamine isothiocyanate (phalloidin-TRITC, Sigma) in a ratio of 1:4. Actin polymerization is initiated by adding one-tenth of the sample volume of a 10-fold concentrated F-buffer (20 mM Tris, 20 mM $MgCl_2$, 2 mM $CaCl_2$, 2 mM dithiothreitol and 1 M KCl). Recombinant I-plastin is reported to bundle actin filaments in the absence, and not in the presence, of calcium. Accordingly, calcium-free actin preparation and F-buffer are used for I-plastin experiments.

INSTRUMENTS AND PROCESSING

All data are acquired on a Zeiss Axiovert 200 inverted microscope with a ×100 oil objective with a numerical aperture of 1.3. Images are captured at a frame rate of one image per 117 ms with a charge-coupled device camera (C4880-80, Hamamatsu). Image storage and analysis are carried out with the image processing software 'OpenBox'[36]. Silanization of the glass surface of a fluid chamber with dichlorodimethylsilane (Sigma) prevented adsorption of emulsion droplets. To determine the fuzzy diameter, D_B, of an F-actin bundle in a ring geometry, the fluorescence intensity profile along a line perpendicular to the bundle is followed in time. Fluctuations are followed for 5–12 s and the intensity profiles are summed. After equilibration D_B is independent of the sampling time (see the Supplementary Information). The wall of the droplet merely fixes the centre of mass of the ring and does not affect the transverse fluctuations of the bundle. In-plane and out-of-plane transverse fluctuations are equal, confirming that the bundle bending stiffness is isotropic (see the Theory section). Gaussian distributions are fitted to both the instantaneous and the time-averaged fluorescence intensity profiles of the bundle, and the standard deviations, σ_{int} and σ_{avg}, respectively, of the distributions are determined. Because σ_{int} does not contribute to the fluctuation amplitude of the bundle $D_B = \sigma_{avg} - \sigma_{int}$. Bundle length L_B was directly proportional to n and the experimentally determined linear relation was used in the further analysis (see the Supplementary Information).

THEORY

An F-actin bundle behaves like a worm-like chain (WLC) with effective bending stiffness, κ_B, and contour length L_B. The κ_B of a WLC bent into a ring is related to the root-mean-square ring radius, R_c, by $\kappa_B = 0.16R_c^3 k_B T/D_B^2$ (ref. 22). Metropolis Monte Carlo simulations were used to determine the prefactor (0.16) and to confirm that WLCs with transversely isotropic bending stiffness have equal transverse fluctuations in- and out-of-the-plane of the ring. To determine the shear stiffness of the crosslinks, κ_B is calculated theoretically using a fibre-based bundle model[25,27]. The maximal deflection, $w_{B,max}$, of a bundle subject to a unit load in three-point bending with pinned boundary conditions is calculated analytically using an analogous version of equation (11) of ref. 25 and equated with the equivalent displacement of a homogeneous Euler–Bernoulli beam, $\kappa_B = L_B^3/48w_{B,max}$, where

$$w_{B,max} = \frac{L_B^3}{48n\kappa_a} - \frac{k_\parallel d(d+t)\sum_{i=1}^{N} i^2}{Kn^2\kappa_a^2\delta}\left[\frac{L_B^3}{24\beta^2} - \frac{L_B}{2\beta^4} + \frac{\tanh\beta L_B/2}{\beta^5}\right]$$

$$\beta^2 \equiv \left[\frac{k_\parallel}{KEA\delta} + \frac{2k_\parallel d(d+t)\sum_{i=1}^{N} i^2}{Kn\kappa_a\delta}\right]$$

and $K \equiv (1/N)\sum_{k=1}^{N}\sum_{i=k}^{N} i$, where n is the total (odd) number of filaments in 2D and $N \equiv (n-1)/2$. F-actin fibres have stretching stiffness $k_a \equiv EA/L_B$ where $EA = 4.4 \times 10^{-8}$ N (ref. 26) and bending stiffness, $\kappa_a \equiv EI = 7.3 \times 10^{-26}$ N m^2 (ref. 37), with diameter $d = 5$ nm corresponding to an effective E of 2 GPa. The total number of fibres in this 2D theory is related to the number of fibres in 3D by $n_{(3D)} = n_{(2D)}^2$, and the corresponding 3D bundle bending stiffness is related to the 2D bundle bending stiffness by $\kappa_{B(3D)} = n_{(2D)}\kappa_{B(2D)}$. δ is the axial spacing between crosslinks and t is the interfilament spacing, taken to be 10 and 35 nm for fascin/plastin and α-actinin, respectively[24,38,39]. δ is calculated assuming ABP–actin chemical equilibrium using $\delta = 38 \times 10^{-9}/\theta$ m, where $\theta = c_{ABP}/(K_d + c_{ABP})$ is the fraction of bound crosslink sites, K_d is the equilibrium dissociation constant for the relevant ABP binding to F-actin bundles ($K_d = 0.5$ μM) and c_{ABP} is the ABP concentration, which is confirmed to be independent of finite-size effects. The minimum mean axial spacing between crosslinks, $\delta_{max} = 38$ nm, corresponds to hexagonally packed F-actin bundles with fully saturated binding sites. The only unknown parameter in the model, $k_\parallel$, is used to fit the experimental κ_B data uniquely for each ABP crosslink examined.

Received 24 April 2006; accepted 24 July 2006; published 20 August 2006.

References

1. Borisy, G. G. & Svitkina, T. M. Actin machinery: Pushing the envelope. *Curr. Opin. Cell Biol.* **12,** 104–112 (2000).
2. Mogilner, A. & Rubinstein, B. The physics of filopodial protrusion. *Biophys. J.* **89,** 782–795 (2005).
3. Atilgan, E., Wirtz, D. & Sun, X. S. Mechanics and dynamics of actin-driven thin membrane protrusions. *Biophys. J.* **90,** 65–76 (2006).
4. Sanger, J. W., Sanger, J. M. & Jockusch, B. M. Differences in the stress fibers between fibroblasts and epithelial-cells. *J. Cell Biol.* **96,** 961–969 (1983).
5. Adams, J. C. Roles of fascin in cell adhesion and motility. *Curr. Opin. Cell Biol.* **16,** 590–596 (2004).
6. Bartles, J. R. Parallel actin bundles and their multiple actin-bundling proteins. *Curr. Opin. Cell Biol.* **12,** 72–78 (2000).
7. Tilney, M. S. *et al.* Preliminary biochemical-characterization of the stereocilia and cuticular plate of hair-cells of the chick cochlea. *J. Cell Biol.* **109,** 1711–1723 (1989).
8. Lin, C. S., Shen, W. Y., Chen, Z. P., Tu, Y. H. & Matsudaira, P. Identification of I-Plastin, a human fimbrin isoform expressed in intestine and kidney. *Mol. Cell. Biol.* **14,** 2457–2467 (1994).
9. Kureishy, N., Sapountzi, V., Prag, S., Anilkumar, N. & Adams, J. C. Fascins, and their roles in cell structure and function. *BioEssays* **24,** 350–361 (2002).
10. Bausch, A. R. & Kroy, K. A bottom-up approach to cell mechanics. *Nature Phys.* **2,** 231–238 (2006).
11. Gardel, M. L. *et al.* Elastic Behavior of cross-linked and bundled actin networks. *Science* **304,** 1301–1305 (2004).
12. Storm, C., Pastore, J. J., MacKintosh, F. C., Lubensky, T. C. & Janmey, P. A. Nonlinear elasticity in biological gels. *Nature* **435,** 191–194 (2005).
13. Kis, A. *et al.* Reinforcement of single-walled carbon nanotube bundles by intertube bridging. *Nature Mater.* **3,** 153–157 (2004).
14. Kovar, D. R. & Pollard, T. D. Insertional assembly of actin filament barbed ends in association with formins produces piconewton forces. *Proc. Natl Acad. Sci. USA* **101,** 14725–14730 (2004).
15. Do, Z. P. *et al.* Mechanosensory function of microvilli of the kidney proximal tubule. *Proc. Natl Acad. Sci. USA* **101,** 13068–13073 (2004).
16. Hudspeth, A. J. & Jacobs, R. Stereocilia mediate transduction in vertebrate hair-cells. *Proc. Natl Acad. Sci. USA* **76,** 1506–1509 (1979).
17. Cotton, J. & Grant, W. Computational models of hair cell bundle mechanics: II. Simplified bundle models. *Hear. Res.* **197,** 105–111 (2004).
18. Howard, J. & Ashmore, J. F. Stiffness of sensory hair bundles in the sacculus of the frog. *Hear. Res.* **23,** 93–104 (1986).
19. Tilney, L. G., Egelman, E. H., Derosier, D. J. & Saunders, J. C. Actin-filaments, stereocilia, and hair-cells of the bird cochlea II. Packing of actin-filaments in the stereocilia and in the cuticular plate and what happens to the organization when the stereocilia are bent. *J. Cell Biol.* **96,** 822–834 (1983).
20. Shin, J. H., Mahadevan, L., So, P. T. & Matsudaira, P. Bending stiffness of a crystalline actin bundle. *J. Mol. Biol.* **337,** 255–261 (2004).
21. Claessens, M. M. A. E., Tharmann, R., Kroy, K. & Bausch, A. R. Microstructure and viscoelasticity of confined semiflexible polymer networks. *Nature Phys.* **2,** 186–189 (2006).
22. Odijk, T. DNA in a liquid-crystalline environment: Tight bends, rings, supercoils. *J. Chem. Phys.* **105,** 1270–1286 (1996).
23. Le Goff, L., Hallatschek, O., Frey, E. & Amblard, F. Tracer studies on F-actin fluctuations. *Phys. Rev. Lett.* **89,** 258101 (2002).
24. Volkmann, N., DeRosier, D., Matsudaira, P. & Hanein, D. An atomic model of actin filaments cross-linked by fimbrin and its implications for bundle assembly and function. *J. Cell Biol.* **153,** 947–956 (2001).
25. Tolomeo, J. A. & Holley, M. C. Mechanics of microtubule bundles in pillar cells from the inner ear. *Biophys. J.* **73,** 2241–2247 (1997).
26. Kojima, H., Ishijima, A. & Yanagida, T. Direct measurement of stiffness of single actin-filaments with and without tropomyosin by in-vitro nanomanipulation. *Proc. Natl Acad. Sci. USA* **91,** 12962–12966 (1994).
27. Bathe, M., Heussinger, C., Claessens, M. M. A. E., Bausch, A. R. & Frey, E. Mechanics of nanofiber bundles. Preprint at <http://arxiv.org/abs/q-bio.BM/0607040> (2006).
28. Hosek, M. & Tang, J. X. Polymer-induced bundling of F actin and the depletion force. *Phys. Rev. E* **69,** 051907 (2004).
29. Tharmann, R., Claessens, M. M. A. E. & Bausch, A. R. Micro- and macrorheological properties of actin networks effectively crosslinked by depletion forces. *Biophys. J.* **90,** 2622–2627 (2006).
30. Li, H. B. *et al.* Reverse engineering of the giant muscle protein titin. *Nature* **418,** 998–1002 (2002).
31. Schlierf, M. & Rief, M. Temperature softening of a protein in single-molecule experiments. *J. Mol. Biol.* **354,** 497–503 (2005).
32. Dietz, H. & Rief, M. Protein structure by mechanical triangulation. *Proc. Natl Acad. Sci. USA* **103,** 1244–1247 (2006).
33. Craig, S. W., Lancashire, C. L. & Cooper, J. A. Preparation of smooth-muscle alpha-actinin. *Methods Enzymol.* **85,** 316–321 (1982).
34. Spudich, J. A. & Watt, S. Regulation of rabbit skeletal muscle contraction. 1. Biochemical studies of interaction of tropomyosin-troponin complex with actin and proteolytic fragments of myosin. *J. Biol. Chem.* **246,** 4866–4871 (1971).
35. Limozin, L., Barmann, M. & Sackmann, E. On the organization of self-assembled actin networks in giant vesicles. *Eur. Phys. J. E* **10,** 319–330 (2003).
36. Schilling, J., Sackmann, E. & Bausch, A. R. Digital imaging processing for biophysical applications. *Rev. Sci. Instrum.* **75,** 2822–2827 (2004).
37. Gittes, F., Mickey, B., Nettleton, J. & Howard, J. Flexural rigidity of microtubules and actin-filaments measured from thermal fluctuations in shape. *J. Cell Biol.* **120,** 923–934 (1993).

38. Edwards, R. A. & Bryan, J. Fascins, a family of actin bundling proteins. *Cell Motil. Cytoskeleton* **32,** 1–9 (1995).
39. Tang, J. H., Taylor, D. W. & Taylor, K. A. The three-dimensional structure of alpha-actinin obtained by cryoelectron microscopy suggests a model for $Ca2^{+}$-dependent actin binding. *J. Mol. Biol.* **310,** 845–858 (2001).

Acknowledgements

We thank M. Rusp for actin preparation and M. Schlierf for his help with protein expression and purification. F. Rivero and D. Vignjevic are acknowledged for the kind gifts of recombinant I-plastin and fascin plasmids, respectively. The authors are grateful for useful discussions with C. Heussinger and M. Rief. This work was supported by the DFG (SFB-413) and the Fonds der Chemischen Industrie.
Correspondence and requests for materials should be addressed to A.R.B.
Supplementary Information accompanies this paper on www.nature.com/naturematerials.

Competing financial interests

The authors declare that they have no competing financial interests.